Int. J. Heat Mass Transfer. Vol. 26, No. 4, pp. 509–519, 1983
Printed in Great Britain

0017–9310/83/040509–11 $03.00/0

A STATISTICAL ANALYSIS OF SATURATED NUCLEATE BOILING ALONG A HEATED WIRE

D. D. PAUL
Battelle Memorial Institute, Columbus, OH 43201, U.S.A.

and

S. I. ABDEL-KHALIK
Dept. of Nuclear Engineering, University of Wisconsin, Madison, WI 53706, U.S.A.

(*Received* 15 *April* 1982 *and in revised form* 30 *July* 1982)

Abstract—Bubble dynamics for saturated nucleate boiling of water on an electrically heated platinum wire at atmospheric pressure have been photographed using a high-speed movie camera. The average number density of active nucleation sites has been found to increase linearly with the boiling heat flux. In addition, the frequency distribution of bubble departure diameters has been found to be well represented by an asymptotic expansion of the normal frequency function. These data have been used to determine the relative contributions to the boiling heat flux of latent heat transport by vapor bubbles, natural convection, and 'enhanced convection' heat transfer.

NOMENCLATURE

a, exponent;
a_J, correlation constant for the average heat removal per bubble, $d\langle J\rangle/dq$ [s m^{-2}];
a_N, correlation constant for the average number density of active nucleation sites, $d\langle N\rangle/dq$ [m W^{-1}];
b_F, correlation constant for the average bubble departure frequency per nucleation site;
b_J, correlation constant for the average heat removal per bubble [J];
b_N, correlation constant for the average number density of active nucleation sites, [m^{-1}];
C_D, normalization constant for the frequency distribution of bubble departure diameters [s^{-1}];
D, bubble departure diameter [m];
$\langle D\rangle$, average bubble departure diameter [m];
D_W, diameter of heated wire [m];
f_C, fraction of the heated surface available for convection heat transfer;
f_g, average fractional chord length of a spherical bubble in contact with the heated surface;
f_l, fractional number of bubble diameters beyond the perimeter of the bubble which experience agitation;
f_{FC}, fraction of the heated surface available for forced convection heat transfer;
f_{NC}, fraction of the heated surface not occupied by bubbles;
$F(D)$, frequency distribution function defined such that $F(D)\,dD$ is the number of bubbles per nucleation site leaving the heated surface per unit time with diameters between D and $D+dD$ [s^{-1} m^{-1}];
$\langle F\rangle$, average bubble departure frequency per nucleation site [s^{-1}];
$\mathscr{F}(\theta)$, unit square wave as shown in Fig. 15;
H_k, the kth Hermite polynomial;
i_{fg}, the latent heat of vaporization [J kg^{-1}];
$\langle J\rangle$, average heat removal per bubble [J];
k, thermal conductivity of liquid, [W m^{-1} K^{-1}];
m, correlation constant exponent for the average bubble departure frequency per nucleation site;
N, number density of active nucleation sites [m^{-1}];
$\langle N\rangle$, average number density of active nucleation sites [m^{-1}];
Nu, Nusselt number;
Nu_0, forced convection Nusselt number evaluated at $\langle V_0\rangle$;
q, nucleate boiling heat flux [W m^{-2}];
q_0, onset of nucleate boiling heat flux [W m^{-2}];
q_{LH}, the latent heat flux contribution to the total heat flux [W m^{-2}];
q_{NC}, the natural convection heat flux contribution to the total heat flux [W m^{-2}];
q_{FC}, the forced convection or 'enhanced convection' heat flux contribution to the total heat flux [W m^{-2}];
Ra, Rayleigh number;
Re, Reynolds number;
T, average temperature of the platinum wire [K];
T_0, bulk temperature of the liquid [K];
U_D, standard normal variable of bubble departure diameters;

U_N, standard normal variable of active nucleation site density;
$U(x,\theta)$, velocity distribution corresponding to a step change boundary condition, equation (44);
V, bubble velocity used to evaluate forced convection heat transfer;
$V(x,\theta)$, velocity distribution corresponding to a square wave boundary condition, equation (40);
V_0, velocity defined by equation (35);
$\langle V_0 \rangle$, time averaged velocity at $x = 0$;
x, horizontal distance from edge of bubble;
x_0, the distance over which the Nusselt number is averaged.

Greek symbols

$\alpha_0, \alpha_1, \alpha_2, \alpha_3, \alpha_4, \alpha_6$, functions of the skewness and kurtosis coefficients defined by equations (19)–(24);
$\beta_0, \beta_1, \beta_2, \beta_3$, function of the average bubble departure diameter and the standard deviation of bubble departure diameters as defined by equations (25)–(28) [m^3];
γ_1, skewness coefficient;
γ_2, kurtosis coefficient;
θ, time;
$\langle \theta \rangle$, the sum of the average growth time and the average waiting period;
$\langle \theta_g \rangle$, average growth time during which the bubble is at the heated surface [s];
$\langle \theta_w \rangle$, average waiting period before a bubble starts to grow [s];
μ_3, third moment about the mean of the experimental data [m^3];
μ_4, fourth moment about the mean of the experimental data [m^4];
ρ_v, density of vapor [kg m^{-3}];
ν, kinematic viscosity;
σ_D, standard deviation of bubble departure diameters [m];
σ_N, standard deviation of active nucleation site density [m^{-1}];
ϕ, normal frequency function;
$\phi^{(k)}$, kth derivative of the normal frequency function.

INTRODUCTION

EARLY studies on the mechanism of nucleate boiling heat transfer have contended that the latent heat transported by vapor bubbles contributes only a few percent of the total heat flux [1–3]. However, these studies, which involve highly subcooled boiling, ignore condensation from the top of the bubbles as they grow into the subcooled liquid. When this mass transfer mechanism was taken into account, Robin and Snyder [4] were able to show that latent heat transport accounted for almost all of the heat transferred in these experiments. For saturated nucleate pool boiling, Rallis and Jawurek [5] found latent heat transport to be significant at all heat fluxes. Despite these findings, many recent publications still downplay the importance of latent heat transport.

With vapor bubbles intermittently growing and departing from the heated surface, nucleate boiling is a transient phenomenon. Since the bubble departure frequency is high ($\sim 100\,s^{-1}$), one is generally interested in the time-averaged values of heat flux. However, the statistical variations in the bubble dynamics must be taken into account in order to accurately calculate the latent heat component. For boiling on a wire, the latent heat component of the heat flux is given by

$$q_{LH} = \frac{1}{\pi D_w} \langle N \rangle \langle F \rangle \langle J \rangle \quad (1)$$

where $\langle N \rangle$ is the average number of active nucleation sites per unit length, $\langle F \rangle$ is the average bubble departure frequency per nucleation site, and $\langle J \rangle$ is the average heat removal per bubble. The primary objectives of this research have been to experimentally measure each of these three average quantities as a function of the boiling heat flux. These are then used to determine how the relative latent heat contribution changes with heat flux. This component is expected to dominate at high heat fluxes. Indeed, at the critical heat flux, all the heat transferred from the surface is due solely to the latent heat flux.

Convection from that portion of the heated surface not occupied by bubbles accounts for the remainder of the heat flux. This is divided into two components, viz. natural convection and 'enhanced convection'. At heat fluxes lower than the onset of nucleate boiling, all of the heat transferred is due solely to natural convection. Natural convection continues to dominate at low nucleate boiling heat fluxes.

The enhanced convection component is associated with agitation and mixing caused by vapor bubbles growing and departing from the heated surface. It will be shown that over the entire range of nucleate boiling heat fluxes, this component will always be less than at least one of the other two components. Yet, in contradiction to the present results, the enhanced convection mode of heat transfer is often considered to be the dominant mode.

EXPERIMENTAL APPARATUS AND PROCEDURE

A schematic diagram of the experimental apparatus used in this investigation is shown in Fig. 1. At the beginning of a run, distilled water is placed in the degassing and preheating vessel. A vacuum pump connected to the vessel removes dissolved gases in solution while a constant temperature bath surrounding the vessel brings the water temperature up to near saturation. After the water has been sufficiently degassed and preheated (~ 1 h), it is transferred to the boiling vessel (Fig. 2). Here it is heated to saturation using two adjustable immersion heaters and a hot plate.

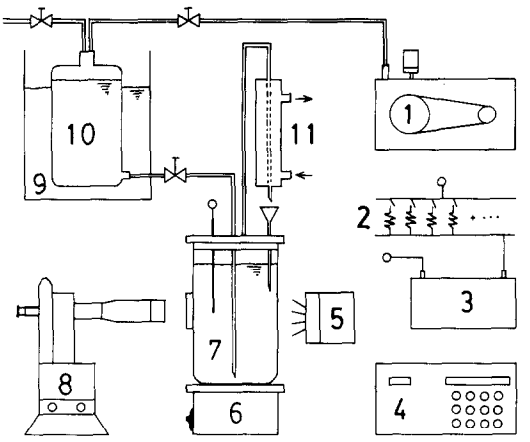

FIG. 1. Schematic diagram of the experimental apparatus and associated equipment: (1) Vacuum pump, (2) resistors, (3) batteries, (4) data logger, (5) photo light, (6) hot plate, (7) boiling vessel, (8) high speed camera or 35 mm camera, (9) constant temperature bath, (10) degassing and preheating vessel, (11) condenser.

The water is kept at saturation conditions for about 30 min before any data are recorded. A condenser located above the boiling vessel condenses any water vapor and returns it back to the test vessel. This prevents changes in water level during the experiment.

Boiling takes place along an electrically heated platinum wire 0.30 mm in diameter, 30.0 mm long submerged at a depth of 70 mm in the water pool. Power is supplied to the platinum wire by three 6 V lead–acid batteries connected in parallel. A group of switched power resistors allow the current, and, therefore, the heat flux, to be precisely controlled. The highest power level is set initially, and subsequent tests are run at progressively lower power levels.

Details of the boiling vessel and associated equipment are shown in Fig. 2. The vessel is a 4000 ml Pyrex beaker fitted with a flat optical window to allow observation and photography of the heated wire. The top of the vessel is sealed by a 1 in. thick phenolic plate. The wire is clamped between two 6.4 mm diameter brass electrodes which penetrate through the vessel cover. The current flowing through the wire is measured by means of a calibrated shunt. The voltage drop across the wire, along with the current, are used to determine the power dissipated, i.e. heat flux, and wire resistance. The later is used to determine the average wire temperature using the temperature–resistance relationship for the wire [6].

The bulk temperature of the liquid is measured using two thermistors (Yellow Spring Instrument Co. type 44301 composite). One of the thermistors is placed directly above the heated wire while the other is placed near the center of the boiling vessel. At saturation conditions, the difference between the two thermistor readings is less than 0.2°C.

At each power level, the thermistor outputs, along with the wire voltage drop and current are recorded using a computerized data logger (Dynatech model 6200) programmed to scan the channels every 10 s. After steady-state conditions are reached, the data are recorded and power is reduced to the next value. The nucleate boiling curve is shown in Fig. 3.

At a given heat flux, bubble dynamics along the entire heated surface are photographed using a high speed movie camera (HYCAM 16 mm camera manufactured by Redlake Corp.). Time markings are automatically placed on the film every millisecond. A film speed of 6400 frames/s has been used in all the experiments. After developing, the films are analyzed using a stop-action 16 mm movie projector (Lafayette Instrument Co. model AAP-200T). Successive frames are individually viewed to determine the number density of active nucleation sites, the bubble departure diameters, and bubble departure frequencies.

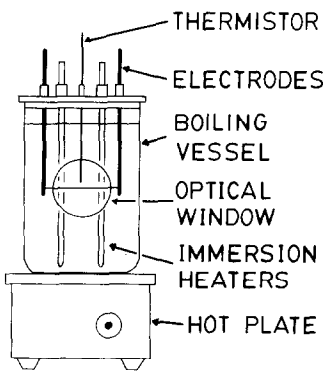

FIG. 2. The boiling vessel and associated equipment.

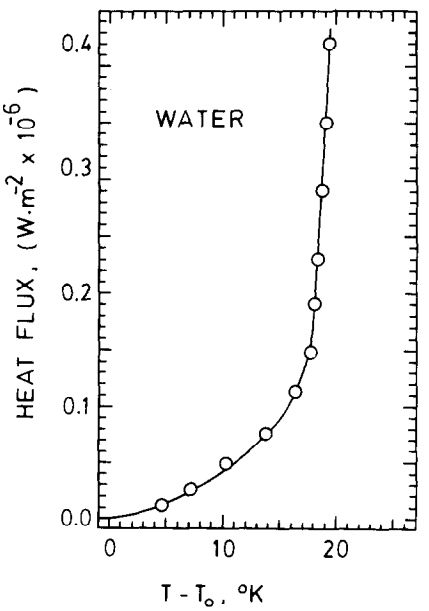

FIG. 3. The nucleate boiling curve for distilled water boiling on a platinum wire.

EXPERIMENTAL RESULTS

In order to determine the latent heat contribution to the total heat flux as given by equation (1), the problem reduces to finding the average number density of active nucleation sites $\langle N \rangle$, the average bubble departure frequency per nucleation site $\langle F \rangle$, and the average heat removal per bubble $\langle J \rangle$. Each of these terms must be determined as a function of the total heat flux.

Active nucleation site density

When analyzing successive frames on the film, a nucleation site is considered active as soon as a bubble appears on the heated surface and is considered inactive the moment the bubble departs from the surface. The time markings on the film make it possible to determine the number density of active nucleation sites as a function of time. Some sections of the heated surface have nucleation sites which are almost always active, whereas other sections have sites which are only sporadically active. Most of the time the individual nucleation sites behave independently of each other, although occasionally interference between adjacent nucleation sites may take place.

By analyzing the movie picture for the entire heated surface, the number density of active nucleation sites at each successive frame can be determined. When considered together, a normal distribution of active nucleation sites is observed. For a particular boiling heat flux, this distribution is given by

$$\phi(U_N) = \frac{1}{(2\pi)^{1/2}} \exp[-U_N^2/2] \tag{2}$$

where U_N is the standard normal variable given by

$$U_N = \frac{N - \langle N \rangle}{\sigma_N}. \tag{3}$$

The normal distributions obtained at four different heat fluxes are shown in Fig. 4. At any given heat flux

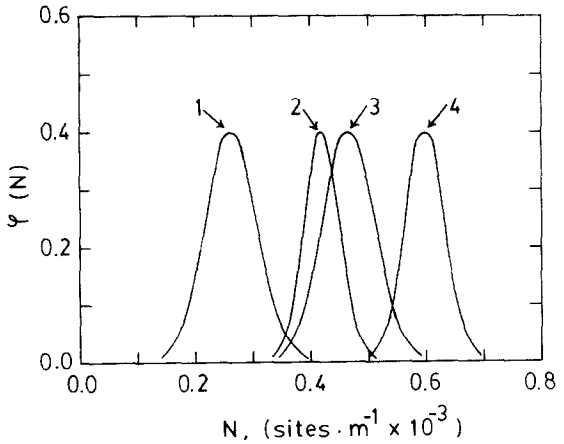

FIG. 4. The distributions of active nucleation site densities at four different boiling heat fluxes: (1) 0.230×10^6 W m^{-2}, (2) 0.352×10^6 W m^{-2}, (3) 0.396×10^6 W m^{-2}, (4) 0.515×10^6 W m^{-2}.

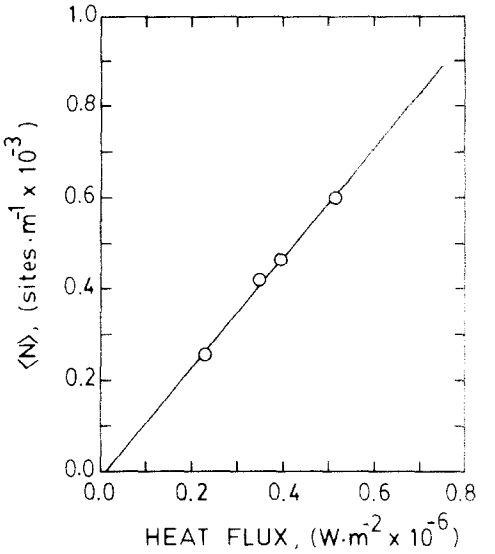

FIG. 5. The average number density of active nucleation sites as a function of the boiling heat flux for water boiling on a platinum wire.

there is a wide variation in the active nucleation site density. Therefore, a large number of frames (~ 1000) need to be analyzed in order to accurately predict the distribution, and hence, the mean number density of active nucleation sites.

When the mean number density of active nucleation sites is plotted as a function of the boiling heat flux (Fig. 5) the data can be represented by the linear relationship

$$\langle N \rangle = (a_N)q + b_N \tag{4}$$

where the slope $a_N = (d\langle N \rangle/dq) = 1.207 \times 10^{-3}$ m W^{-1}, and the intercept, $b_N = 15.74$ m^{-1}, are determined from a least squares fit of the experimental data.

The heat flux at the onset of nucleate boiling q_0 can be determined as the point where the number density of active nucleation sites equals zero. This condition gives

$$q_0 = \frac{-b_N}{a_N}. \tag{5}$$

For our experimental results, the onset of nucleate boiling occurs at a heat flux of 0.0130×10^6 W m^{-2}.

Bubble departure diameter frequency distributions

Perhaps the area where previous analyses have been most inadequate is in the determination of the frequency distribution of bubble departure diameters. Most previous investigators [7–9] have correlated their experimental data in the form

$$D\langle F \rangle^a = \text{constant}. \tag{6}$$

This expression was found to be inadequate especially for small bubble diameters.

Using the films obtained for the entire boiling surface, the departure diameter for each bubble leaving the heated surface has been measured. If two bubbles

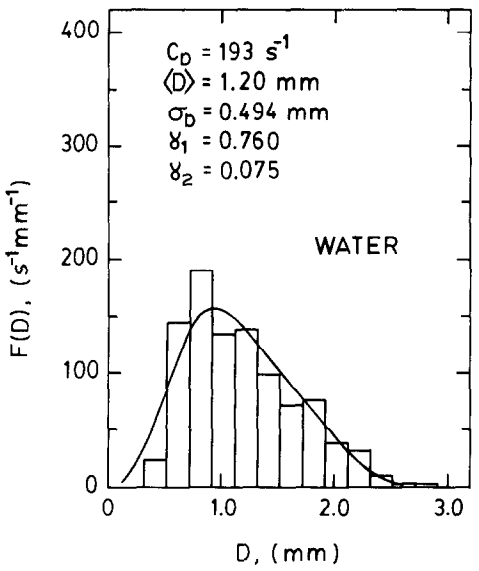

FIG. 6. The frequency distribution of bubble departure diameters at a boiling heat flux of 0.230×10^6 W m^{-2}.

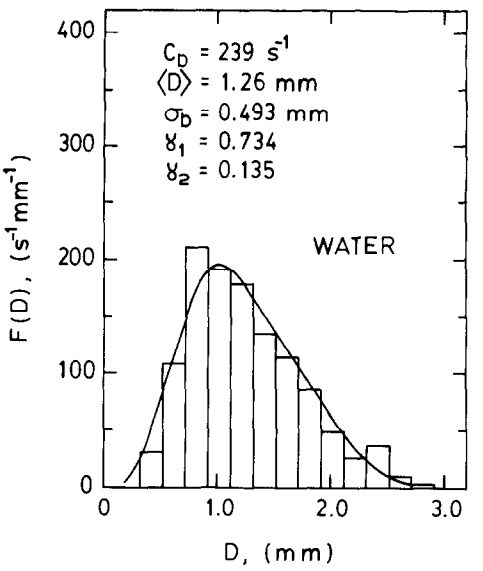

FIG. 8. The frequency distribution of bubble departure diameters at a boiling heat flux of 0.396×10^6 W m^{-2}.

combine before leaving the surface, their departure diameters are measured separately at the moment just before they combine. By taking these measurements over a known period of time, typically 1000 frames, a distribution of bubble departure diameters is obtained. The frequency distribution function is defined such that $F(D)\,dD$ is the number of bubbles leaving the surface per nucleation site per unit time with diameters between D and $D+dD$.

Frequency distributions are shown in Figs. 6, 7, 8 and 9 for water boiling on a platinum wire at heat fluxes of 0.230×10^6, 0.352×10^6, 0.396×10^6 and 0.515×10^6 W m^{-2} respectively. The histogram portion of the graphs represent actual experimental data. The curves drawn on these plots are fitted asymptotic expansions of the normal frequency function [10, 11] defined by

$$F(D) = \frac{C_D}{\sigma_D}\left\{\phi(U_D) - \left[\frac{\gamma_1}{6}\phi^{(3)}(U_D)\right] + \left[\frac{\gamma_2}{24}\phi^{(4)}(U_D) + \frac{\gamma_1^2}{72}\phi^{(6)}(U_D)\right]\right\} \quad (7)$$

where

$$U_D = \frac{D - \langle D\rangle}{\sigma_D} \quad (8)$$

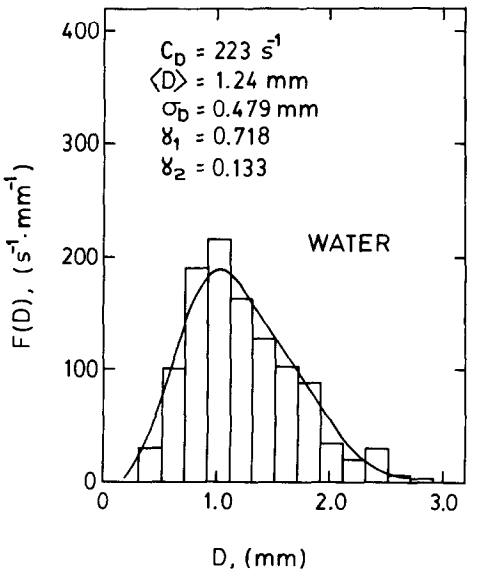

FIG. 7. The frequency distribution of bubble departure diameters at a boiling heat flux of 0.352×10^6 W m^{-2}.

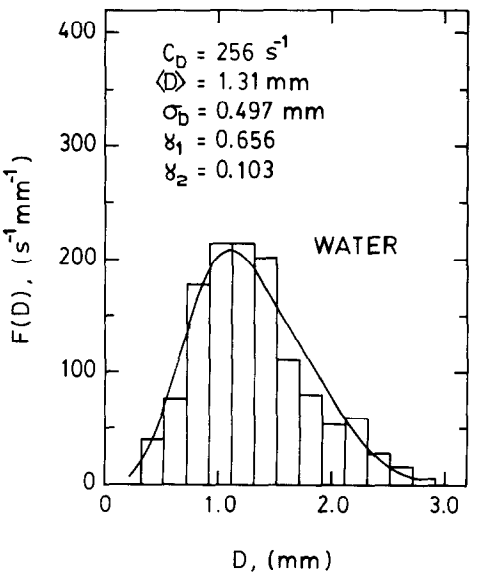

FIG. 9. The frequency distribution of bubble departure diameters at a boiling heat flux of 0.515×10^6 W m^{-2}.

and the derivatives of the normal frequency function are

$$\phi^{(k)}(U_D) = \left(\frac{-1}{\sqrt{2}}\right)^k H_k\left(\frac{U_D}{\sqrt{2}}\right)\phi(U_D) \tag{9}$$

where H_k is the kth Hermite polynomial. The coefficients γ_1 and γ_2 are the skewness and kurtosis coefficients, respectively, defined by

$$\gamma_1 = \frac{\mu_3}{\sigma_D^3} \tag{10}$$

and

$$\gamma_2 = \frac{\mu_4}{\sigma_D^4} - 3 \tag{11}$$

where μ_3 and μ_4 are the third and fourth moments about the mean of the experimental data. Values of C_D, $\langle D\rangle$, σ_D, γ_1 and γ_2 are given on each plot.

The average bubble departure frequency per nucleation site is then

$$\langle F\rangle = \int_0^{+\infty} F(D)\,\mathrm{d}D. \tag{12}$$

The frequency distribution function is defined such that the above integral is equal to the normalization constant C_D to within an error of less than 1%. This slight error arises because the normal limits on the integration extend from $-\infty$ to $+\infty$. The average bubble diameter is about three standard deviations from the origin so only a small error is introduced by choosing the lower limit to be 0 instead of $-\infty$.

Although the area under the curve, i.e. the average bubble departure frequency, changes with the heat flux the overall shape of the distribution remains the same. The shapes of the curves are determined by the standard deviation, skewness coefficient and the kurtosis coefficient. These parameters are independent of the boiling heat flux, and therefore depend only on the fluid–surface combination. Since the bubble departure diameters and frequencies depend on the size and shape of the nucleation sites [12, 13], it is not altogether surprising that the statistical parameters describing the shape of the distribution function also characterize the boiling surface. Using our experimental data for water boiling on a platinum surface, the average values of these parameters are: $\langle\sigma_D\rangle = 0.491$ mm, $\langle\gamma_1\rangle = 0.717$, and $\langle\gamma_2\rangle = 0.112$.

Values of the average bubble departure diameter $\langle D\rangle$ as a function of the boiling heat flux are shown in Fig. 10. The value of $\langle D\rangle$ increases very slowly as the boiling heat flux increases. This is physically reasonable since the average wire surface temperature increases only slightly as the boiling heat flux increases (Fig. 3). The straight line drawn through the data points in Fig. 10, obtained by a least squares fit, has a slope of 0.3874×10^{-9} m^3 W^{-1} and an intercept of 1.108×10^{-3} m.

The average bubble departure frequency per nucleation site $\langle F\rangle$ increases dramatically with the boiling heat flux. Figure 11 is a plot of $\langle F\rangle$ against the difference between the boiling heat flux q and the onset heat flux q_0. The data can be correlated by the expression

$$\langle F\rangle = b_F(q-q_0)^m. \tag{13}$$

The constants $b_F = 2.843$ and $m = 0.3434$ have been obtained from a least squares fit of the data where $\langle F\rangle$ has units of s^{-1} and the heat fluxes have units of W m^{-2}. The fact that after a bubble leaves the heated surface the thermal boundary layer grows more quickly at higher heat fluxes accounts for the dramatic change in the bubble departure frequency even though the average surface temperature of the wire does not appreciably change.

By definition, the average time period for a bubble cycle is

$$\langle\theta\rangle = \frac{1}{\langle F\rangle}. \tag{14}$$

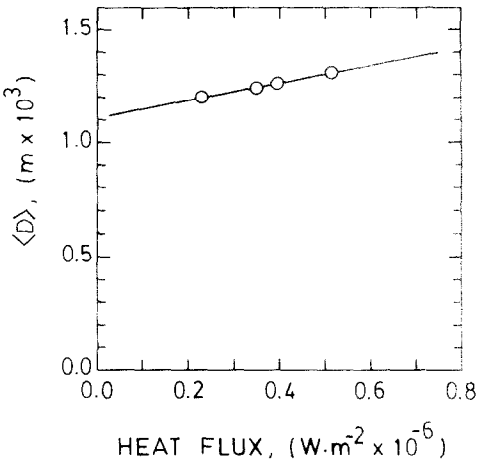

FIG. 10. The average bubble departure diameter as a function of the boiling heat flux for water boiling on a platinum wire.

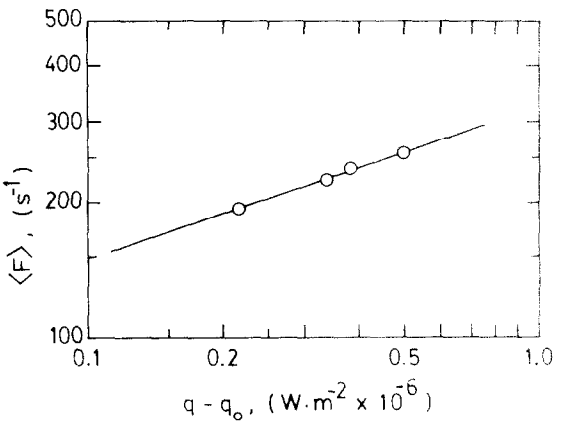

FIG. 11. The average bubble departure frequency per nucleation site as a function of the boiling minus the onset heat flux for water boiling on a platinum wire.

This time period can be divided into the average waiting period $\langle\theta_w\rangle$ before a bubble begins to grow and the average growth period $\langle\theta_g\rangle$ during which a bubble is in contact with the heated surface, where

$$\langle\theta_w\rangle = (1-f_g\langle D\rangle\langle N\rangle)\langle\theta\rangle \tag{15}$$

and

$$\langle\theta_g\rangle = (f_g\langle D\rangle\langle N\rangle)\langle\theta\rangle. \tag{16}$$

Figure 12 shows the average waiting period and the average growth time as a function of the boiling heat flux. The average waiting period continuously decreases as the boiling heat flux increases, whereas the average growth time is zero at the onset of nucleate boiling and increases steadily with the boiling heat flux.

Average heat removal per bubble

The average heat removal per bubble is easily calculated from the frequency distribution of bubble departure diameters as

$$\langle J\rangle = \frac{\rho_v i_{fg}\int_0^{+\infty}\frac{\pi}{6}D^3F(D)\,dD}{\int_0^{+\infty}F(D)\,dD} \tag{17}$$

Substituting equation (7) into the above expression and performing the integration yields

$$\langle J\rangle = \frac{\pi}{6}\rho_v i_{fg}\{[\alpha_0\beta_0]+[\alpha_0\beta_2+\alpha_1\beta_1+\alpha_2\beta_0]^{\frac{1}{2}} + [\alpha_1\beta_3+\alpha_2\beta_2+\alpha_3\beta_1+\alpha_4\beta_0]^{\frac{3}{4}} + [\alpha_3\beta_3+\alpha_4\beta_2+\alpha_6\beta_0]^{\frac{15}{8}} + [\alpha_6\beta_2]^{\frac{105}{16}}\} \tag{18}$$

where

$$\alpha_0 = 1+\frac{\gamma_2}{8}-\frac{15}{72}\gamma_1^2, \tag{19}$$

$$\alpha_1 = \frac{-\gamma_1}{\sqrt{2}}, \tag{20}$$

$$\alpha_2 = \tfrac{5}{4}\gamma_1^2-\frac{\gamma_2}{2}, \tag{21}$$

$$\alpha_3 = \frac{\sqrt{2}}{3}\gamma_1, \tag{22}$$

$$\alpha_4 = \frac{\gamma_2}{6}-\tfrac{5}{6}\gamma_1^2, \tag{23}$$

$$\alpha_6 = \tfrac{1}{9}\gamma_1^2, \tag{24}$$

and

$$\beta_0 = \langle D\rangle^3, \tag{25}$$

$$\beta_1 = 3\sqrt{2}\sigma_D\langle D\rangle^2, \tag{26}$$

$$\beta_2 = 6\sigma_D^2\langle D\rangle, \tag{27}$$

$$\beta_3 = 2\sqrt{2}\sigma_D^3. \tag{28}$$

For the special case of a gaussian distribution, i.e. $\gamma_1 = \gamma_2 = 0$, equation (18) simplifies to

$$\langle J\rangle = \frac{\pi}{6}\langle D\rangle^3\rho_v i_{fg}\left[1+\left(\frac{\sqrt{3}\sigma_D}{\langle D\rangle}\right)^2\right]. \tag{29}$$

Figure 13 shows the average heat removed per bubble, as calculated from the experimental data, plotted as a function of the boiling heat flux. These data can be represented by the linear relationship

$$\langle J\rangle = (a_J)q+b_J \tag{30}$$

where the slope $a_J = \mathrm{d}\langle J\rangle/\mathrm{d}q = 1.57\times10^{-9}\ \mathrm{s\,m^2}$, and the intercept, $b_J = 1.504\times10^{-3}$ J, have been obtained from a least squares fit of the data. Values of $\langle J\rangle$ calculated from equation (18) are within 0.1% of the experimentally calculated values; use of the simpler equation (29) underestimates $\langle J\rangle$ by about 3–4%.

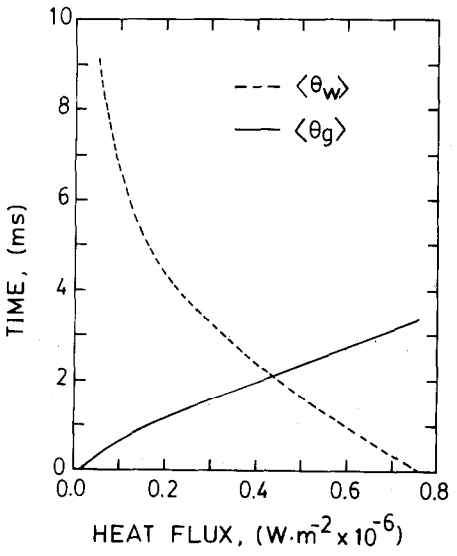

FIG. 12. The bubble cycle average waiting period and average growth time as a function of the boiling heat flux.

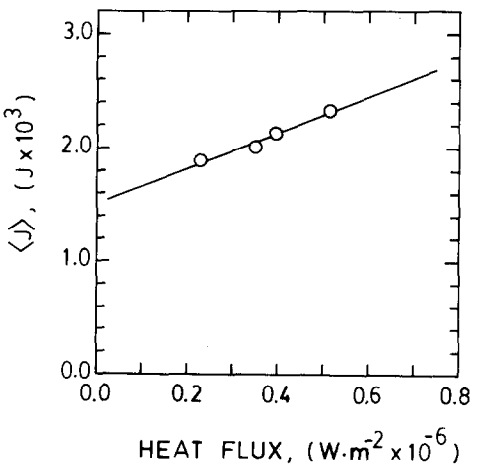

FIG. 13. The average heat removal per bubble as a function of the boiling heat flux for water boiling on a platinum wire.

DISCUSSION

The latent heat contribution to the total heat flux

The experimentally determined correlations for the average number density of active nucleation sites [equation (4)], the average bubble departure frequency per nucleation site [equation (13)], and the average heat removal per bubble [equation (30)] may be substituted into equation 1 to determine the latent heat transport contribution to the boiling heat flux. The results of this calculation are shown in Fig. 14. At very low heat fluxes, the latent heat contribution approaches zero because the number density of active nucleation sites goes to zero and the average bubble departure frequency per nucleation site also goes to zero. At very high heat fluxes, the majority of heat transferred is due to latent heat transport. The critical heat flux is defined as the point where the latent heat contribution equals 100% of the observed boiling heat flux. For our experimental apparatus, extrapolation of the data in Fig. 14 yields a critical heat flux of 0.755×10^6 W m^{-2}. This agrees well with the experimentally measured value of 0.72×10^6 W m^{-2} [6].

The natural convection heat flux

The natural convection contribution to the boiling heat flux may be calculated using existing correlations for natural convection heat transfer. However, no reliable correlation exists for the extremely low values of Rayleigh number encountered in our experiment. Hence, a non-linear curve fit of McAdams data [14] for natural convection from horizontal long cylinders with $Ra \leqslant 10^4$ has been performed [6] to obtain:

$$Nu = (1.000)Ra^n \quad (Ra \leqslant 10^4) \tag{31}$$

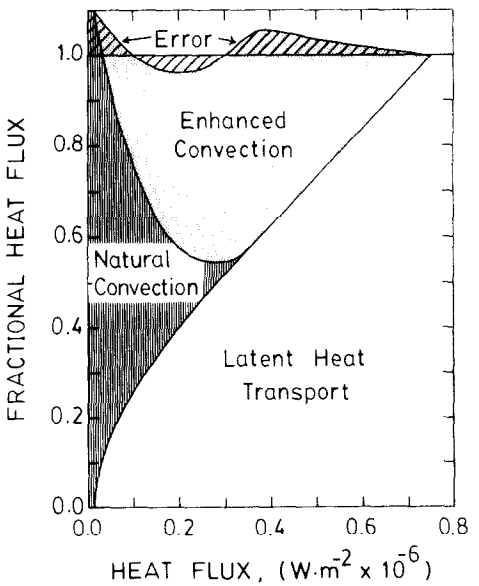

FIG. 14. The relative contribution of the latent heat flux, the natural convection heat flux, and the enhanced convection heat flux to the total heat flux observed in nucleate boiling.

where the exponent n is

$$n = 0.130 + 0.0125 \log (Ra). \tag{32}$$

The natural convection contribution to the heat flux on boiling surfaces is defined as:

$$q_{NC} = \frac{k}{D_w} Nu(T - T_0) f_{NC} \tag{33}$$

where f_{NC} is the fraction of the heated surface experiencing natural convection [equation (52)]. Figure 14 shows the natural convection contribution to boiling heat flux. At heat fluxes lower than the onset of nucleate boiling, all of the heat transferred is due to natural convection. At low boiling heat fluxes, the natural convection term still dominates but latent heat transport becomes increasingly significant. Finally, at high heat fluxes the natural convection heat flux is small compared to the latent heat flux. Furthermore, the fraction of the heated surface not occupied by bubbles approaches zero at the critical heat flux, and this further reduces the natural convection contribution.

The enhanced convection heat flux

The enhanced convection heat flux can be estimated using a forced convection correlation for flow normal to circular cylinders developed by Hilpert [15],

$$Nu = C_1 Re^{C_2} \tag{34}$$

where C_1 and C_2 are constants given in Table 1.

This correlation can be used to obtain an average Nusselt number provided the velocity distribution $V(x, \theta)$ around a growing and departing bubble is known. To estimate the velocity distribution, the velocity field produced during the bubble growth and departure cycle is approximated by that produced by a flat plate moving with velocity

$$V_0 = \frac{\langle D \rangle}{\langle \theta_g \rangle} \tag{35}$$

during the growth interval $\langle \theta_g \rangle$, followed by a waiting period $\langle \theta_w \rangle$ during which the plate is assumed to be at rest. Figure 15 shows the postulated 'bubble' velocity as a function of time.

Han and Griffith [16] found that the velocity field around a sphere pulled from a flat surface extends out to

Table 1. Forced convection correlation constants for flow normal to circular cylinders [15]

Re	C_1	C_2
1–4	0.891	0.330
4–40	0.821	0.385
40–4000	0.615	0.466
4000–40 000	0.174	0.618
40 000–250 000	0.0239	0.805

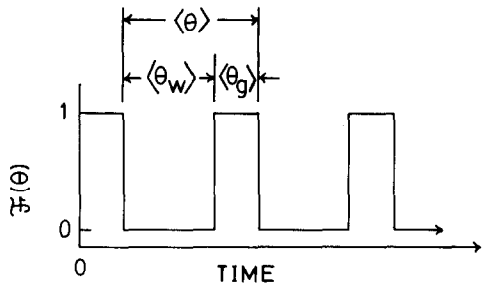

FIG. 15. The postulated bubble velocity as a function of time.

about one sphere diameter from the edge of the sphere, so that

$$V(f_1\langle D\rangle, \theta) = 0 \tag{36}$$

where $f_1 = 1$. For thin wires, one would expect the influence region around a departing bubble to be smaller than that for a flat plate so that f_1 is less than unity.

A momentum balance on the hypothetical system described above yields the following differential equation:

$$\frac{dV}{d\theta} = \nu \frac{d^2V}{dx^2} \tag{37}$$

subject to the initial condition

$$V(x > 0, 0) = 0 \tag{38}$$

and the boundary condition

$$V(0, \theta) = V_0 \mathcal{F}(\theta) \tag{39}$$

where $\mathcal{F}(\theta)$ is given in Fig. 15. Duhamel's theorem is used to solve equation (37) subject to the initial condition (38) and the two boundary conditions (36) and (39). The solution is

$$V(x,\theta) = \sum_{\substack{n=0 \\ n\,\text{even}}}^{\infty} U\left(x, \theta - \frac{n}{2}\langle\theta\rangle\right) - \sum_{\substack{n=1 \\ n\,\text{odd}}}^{\infty} U\left\{x, \theta - \left[\left(\frac{n+1}{2}\right)\langle\theta\rangle - \langle\theta_w\rangle\right]\right\} \tag{40}$$

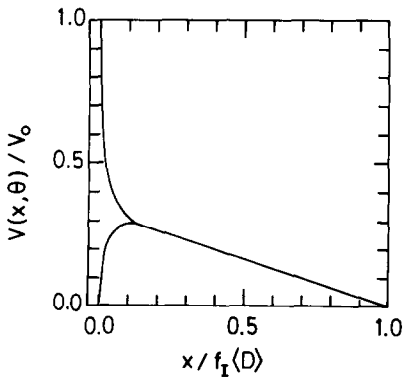

FIG. 16. The upper and lower bounds of the sustained transient solution for $\langle\theta_g\rangle = 1.564$ ms and $\langle\theta_w\rangle = 3.135$ ms.

where

$$\langle\theta\rangle = \langle\theta_g\rangle + \langle\theta_w\rangle \tag{41}$$

and for n even:

$$\left[\frac{n}{2}\langle\theta\rangle\right] < \theta < \left[\frac{n}{2}\langle\theta\rangle + \langle\theta_g\rangle\right] \tag{42}$$

and for n odd:

$$\left[\frac{n+1}{2}\langle\theta\rangle - \langle\theta_w\rangle\right] < \theta < \left[\frac{n+1}{2}\langle\theta\rangle\right]. \tag{43}$$

In the above infinite series, the function $U(x, \theta)$ is given by

$$U(x,\theta) = V_0\left[\left\{1 - \frac{x}{f_1\langle D\rangle}\right\} - \left\{\frac{2}{\pi}\sum_{j=1}^{\infty}\left(\frac{1}{j}\right) \times \sin\frac{j\pi x}{f_1\langle D\rangle}\exp\left[-\left(\frac{j\pi}{f_1\langle D\rangle}\right)^2 \nu\theta\right]\right\}\right]. \tag{44}$$

As an example of a typical calculation, the velocity distributions at $V(x, 500\langle\theta\rangle + \langle\theta_g\rangle)$ and $V(x, 501\langle\theta\rangle)$ (the upper and lower curves, respectively, in Fig. 16) have been calculated for values of $\langle D\rangle$, $\langle\theta_g\rangle$ and $\langle\theta_w\rangle$ corresponding to the bubble parameters at a heat flux of 0.30×10^6 W m^{-2}. These two distributions define the upper and lower bounds of the sustained transient velocity distribution.

If the sustained transient velocity distribution is averaged over a bubble growth and departure cycle, the resulting spatial variation of time-averaged velocity is given by

$$\langle V(x)\rangle = \langle V_0\rangle\left[1 - \frac{x}{f_1\langle D\rangle}\right] \tag{45}$$

where

$$\langle V_0\rangle = \langle D\rangle\langle F\rangle. \tag{46}$$

When this velocity distribution is used to calculate an average Nusselt number, the result is

$$\langle Nu\rangle = \frac{Nu_0}{\left(\frac{x_0}{f_1\langle D\rangle}\right)(1+C_2)}\left[1 - \left(1 - \frac{x_0}{f_1\langle D\rangle}\right)^{1+C_2}\right] \tag{47}$$

where

$$Nu_0 = C_1\left(\frac{\rho_L\langle V_0\rangle D_w}{\mu_L}\right)^{C_2} \tag{48}$$

and x_0 is equal to either $f_1\langle D\rangle$ or one-half the average distance between bubbles, whichever is smaller. The average Nusselt number is weakly dependent on the parameter f_1. A value of $f_1 = 0.65$ results in good agreement between the model and the experimental data. The enhanced convection heat flux is then given by

$$q_{FC} = \frac{k}{D_w}\langle Nu\rangle(T - T_0)f_{FC} \tag{49}$$

where f_{FC} is the fraction of the wire experiencing forced convection [equation (51)].

The fraction of the surface not occupied by vapor bubbles and, therefore, available for convection heat transfer is

$$f_C = 1 - f_g \langle D \rangle \langle N \rangle \quad (50)$$

where f_g is the average fractional chord length of a spherical bubble in contact with the heated surface. This fraction is subdivided into two parts: the forced convection fraction and the natural convection fraction. The forced convection fraction is determined using

$$f_{FC} = (2) f_1 \langle D \rangle \langle N \rangle \quad (51)$$

where f_1 is the fractional number of bubble diameters beyond the edge of the bubble which experience agitation. When f_{FC} is greater than f_C, then f_{FC} is set equal to f_C. This accounts for interference between vapor bubbles at high boiling heat fluxes. The natural convection fraction is obtained by the balance relationship

$$f_{NC} = f_C - f_{FC}. \quad (52)$$

Figure 14 shows the relative contribution of the enhanced convection heat flux over the entire range of nucleate boiling. At very low heat fluxes there are very few active nucleation sites and the average bubble departure frequency is small, so that very little agitation and mixing occurs on the heated surface. At intermediate heat fluxes, agitation and mixing brought about by bubble departure is at a maximum and it is in this region that the enhanced convection contribution reaches its maximum value of about 45% of the total heat flux. Finally, at the highest heat fluxes the bubbles begin to interfere with each other and start to impede the flow of liquid to the heated surface. This explains the decrease in the enhanced convection contribution at the highest heat fluxes. It is worthwhile to note that the enhanced convection heat flux is always less than at least one of the other two components.

CONCLUSIONS

The relative contributions of the three components of the nucleate boiling heat flux have been examined over the entire range between the onset of nucleate boiling and the critical heat flux. Based on the results of this investigation, the following conclusions are made:

(1) The latent heat transport by vapor bubbles dominates at intermediate to high boiling heat fluxes. At the critical heat flux, all of the heat transfer is due to latent heat transport.

Due to the transient nature of bubbles growing and departing from the heated surface, significant statistical variations have been observed in the number density of active nucleation sites and the frequency distribution of bubble departure diameters. These statistical variations must be accurately measured in order to calculate the latent heat transport contribution to the boiling heat flux. For a given fluid–surface combination, the statistical parameters describing the shape of the frequency distribution of bubble departure diameters have been found to be independent of the boiling heat flux, and therefore can be used to characterize the boiling surface.

(2) The natural convection contribution from that portion of the heated surface not occupied by vapor bubbles dominates heat transfer at low boiling heat fluxes.

(3) The enhanced convection component is important at intermediate boiling heat fluxes where agitation and mixing brought about by departing vapor bubbles is the greatest. For the experimental apparatus used, the enhanced convection contribution was always less than at least one of the other components.

Acknowledgements—Financial support by the National Science Foundation (Grant No. ENG 77-21909) and the Wisconsin Alumni Research Foundation is acknowledged.

REFERENCES

1. F. C. Gunther, Photographic study of surface-boiling heat transfer to water with forced convection, *Trans. Am. Soc. Mech. Engrs* **73**, 115–124 (1951).
2. W. M. Rohsenow and J. A. Clark, A study of the mechanism of boiling heat transfer, *Trans. Am. Soc. Mech. Engrs* **73**, 609–620 (1951).
3. K. E. Forster and R. Greif, Heat transfer to a boiling liquid—mechanism and correlations, *J. Heat Transfer* **81**, 43–53 (1959).
4. T. T. Robin and N. W. Snyder, Bubble dynamics in subcooled nucleate boiling based on the mass transfer mechanism, *Int. J. Heat Mass Transfer* **13**, 305–318 (1970).
5. C. J. Rallis and H. H. Jawurek, Latent heat transport in saturated nucleate boiling, *Int. J. Heat Mass Transfer* **7**, 1051–1068 (1964).
6. D. D. Paul, Nucleate boiling in drag-reducing polymer solutions. PhD Thesis, University of Wisconsin, Madison (1982).
7. H. J. Ivey, Relationships between bubble frequency, departure diameter and rise velocity in nucleate boiling, *Int. J. Heat Mass Transfer* **10**, 1023–1040 (1967).
8. B. B. Mikic, W. M. Rohsenow and P. Griffith, On bubble growth rates, *Int. J. Heat Mass Transfer* **13**, 657–666 (1970).
9. R. Cole, Photographic study of boiling in region of critical heat flux, *A.I.Ch.E.Jl* **6**, 533–538 (1960).
10. M. Zelen and N. C. Severo, Probability functions, in *Handbook of Mathematical Functions* (edited by M. Abramowitz and I. A. Stegun), pp. 927–995 (1972).
11. G. A. Korn and T. M. Korn, Mathematical statistics, in *Mathematical Handbook For Scientists and Engineers*, pp. 664–714. McGraw-Hill, New York (1968).
12. M. Shoukri and R. L. Judd, On the influence of surface conditions in nucleate boiling—the concept of bubble flux density, *J. Heat Transfer* **100**, 618–623 (1978).
13. A. K. Chesters, Modes of bubble growth in slow formation regime of nucleate pool boiling, *Int. J. Multiphase Flow* **4**, 279–302 (1978).
14. W. H. McAdams, *Heat Transmission*, pp. 172–176. McGraw-Hill, New York (1954).
15. R. Hilpert, *Forsch. Geb. IngWes.* **4**, 215 (1933).
16. C.-Y. Han and P. Griffith, The mechanism of heat transfer in nucleate pool boiling—part II, *Int. J. Heat Mass Transfer* **8**, 905–914 (1965).

ANALYSE STATISTIQUE DE L'EBULLITION NUCLEEE LE LONG D'UN FIL CHAUFFE

Résumé—Les bulles dans l'ébullition nucléée d'eau saturante sur un fil de platine chauffé électriquement à la pression atmosphérique sont photographiées à l'aide d'une caméra à grande vitesse. La densité moyenne en nombre de sites de nucléation active croît linéairement avec le flux de chaleur. De plus la distribution de fréquence des diamètres de bulles au détachement est bien représentée par un développement asymptotique de la fonction normale. Ces données sont utilisées pour déterminer les contributions relatives, au flux thermique, du transfert de chaleur latente par les bulles de vapeur, de la convection naturelle et de la "convection accrue".

EINE STATISTISCHE ANALYSE DES GESÄTTIGTEN BLASENSIEDENS AN EINEM BEHEIZTEN DRAHT

Zusammenfassung—Es wurde die Blasenbewegung des gesättigten Blasensiedens von Wasser an einem elektrisch beheizten Platindraht bei atmosphärischem Druck mit Hilfe einer Hochgeschwindigkeitskamera fotografiert. Es stellte sich heraus, daß die durchschnittliche Dichte der aktiven Keimstellen proportional mit der Wärmestromdichte des Siedens ansteigt. Darüber hinaus wurde festgestellt, daß die Häufigkeitsverteiling des Blasenabreißdurchmessers gut durch eine asymptotische Annäherung der gewöhnlichen Häufigkeitsfunktion wiedergegeben werden konnte. Diese Daten wurden benutzt, um der relativen Beitrag des latenten Wärmetransports durch Dampfblasen, der freien Konvektion und des Wärmeübergangs bei "erhöhter Konvektion" zur Wämestromdichte beim Sieden zu bestimmen.

СТАТИСТИЧЕСКИЙ АНАЛИЗ ПУЗЫРЬКОВОГО КИПЕНИЯ НА НАГРЕВАЕМОЙ ПРОВОЛОКЕ

Аннотация—С помощью скоростной киносъемки проведено фотографирование процесса роста пузырьков при насыщенном пузырьковом кипении воды на нагреваемой электрическим током платиновой проволоке при атмосферном давлении. Найдено, что средняя плотность активных областей зарождения пузырьков линейно возрастает с увеличением величины теплового потока. Кроме того показано, что распределение отрывных диаметров пузырьков по частоте можно с хорошей точностью описать асимптотическим разложением нормальной частотной функции. На основе полученных данных определен относительный вклад, вносимый в теплоперенос при кипении пузырьками, свободной и вынужденной конвекцией.